


ORIGINAL ARTICLE

Confocal microscopy of telangiectatic capillaries (TelCaps) and other features of microvascular remodeling following branch retinal vein occlusion

Marie Darche^{1,2}  | Anna Verschueren^{1,2} | Daniela Castro Farias¹ | Ysé Borella^{1,2} | Michel Paques^{1,2}

¹Quinze-Vingts Hospital, Institut National de la Recherche Médicale, Direction générale de l'offre de soins, centre d'investigation clinique 1423, Paris, France

²Institut de la Vision, INSERM, UMR968, Paris, France

Correspondence

Michel Paques, Quinze-Vingts Hospital, Institut National de la Recherche Médicale, Direction générale de l'offre de soins, centre d'investigation clinique 1423, 28 Rue de Charenton, 75012 Paris, France. Email: mpaques@15-20.fr

Funding information

Association contre l'OVR; Agence Nationale de la Recherche (ANR-18-IAHU-01 ForeSight)

Abstract

Branch retinal vein occlusion (BRVO) is a frequent retinal vascular disease that may cause extensive microvascular remodeling leading to severe visual impairment. Little is known regarding the histology of non-neovascular microvascular remodeling. Here, we examined by confocal microscopy the structure of retinal microvessels of a donor eye with longstanding BRVO. The post-mortem retina of a 91-year-old woman that had superotemporal BRVO for 2 years was examined by confocal microscopy after anti-collagen IV (collIV), alpha-smooth muscle cell (α SMA), and anti-von Willebrand factor (vWf) immunolabeling. In the retinal quadrant affected by BRVO, extensive vascular remodeling affected all vessels, from arterioles to venules, including the foveal avascular zone. Most affected vessels were either irregularly dilated or, on the opposite, reduced to micrometric-size CollIV positive, vWf negative, nuclear-staining negative strings. Telangiectatic capillaries of various sizes and shapes were seen, the largest one (233 μ m) being located in the parafoveal area. Some telangiectatic capillaries had a thick, multilayered vWf- and CollIV-positive wall, that often occluded the lumen. Other features included double-channeled arterioles. The majority of microvascular abnormalities were devoid of nuclear staining, suggesting extensive loss of endothelial cells. We describe the spectrum of microvascular abnormalities upstream of a longstanding BRVO. This spectrum comprises a large parafoveal telangiectatic capillary corresponding to what has been previously clinically defined as TelCap. The absence of intraluminal nuclear staining in the majority of abnormal vessels raises the hypothesis that the loss of endothelial cells plays a crucial role in the development of the different manifestations of capillary remodeling. The presence of vWF in de-endothelialized vessels suggests deposition of plasma, hence that they may remain perfused. Our work may help to understand the clinical imaging features of TelCaps.

KEYWORDS

capillaries, confocal microscopy, retina, retinal vein occlusion, TelCaps

1 | INTRODUCTION

Branch retinal vein occlusion (BRVO) is an age-related microvascular disease consecutive to a focal interruption of venous flow at an

arteriovenous crossing. Retinal vein occlusions represent a common cause of vascular blindness after diabetic retinopathy, with an age-related prevalence reaching more than 2% after 80 years (Song et al., 2019). The severity of microvascular remodeling, which

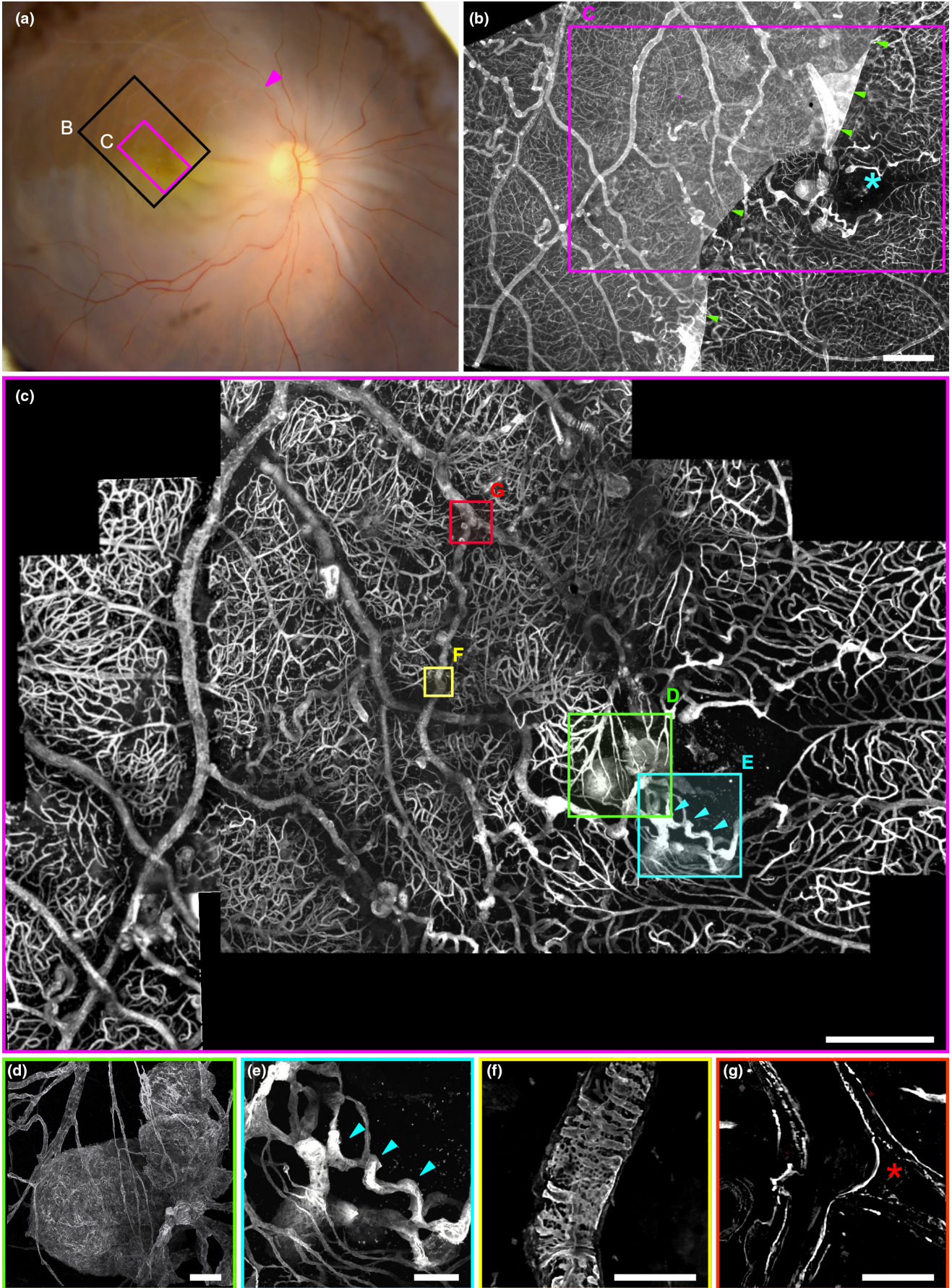


FIGURE 1 (a) Post-mortem fundus photograph of the sample superimposed on the area examined by microscopy. Arrowhead indicates the presumed site of occlusion; areas shown in (b) and (c) are boxed in black and magenta, respectively. (b) Epifluorescence imaging. The blue asterisk marks the foveal avascular zone. The presence of the inner limiting membrane, stained by anticollIV antibodies, partially attached to the macula, explained the lower contrast on the left of the image. (c) Confocal microscopy of the foveal area; localisations of panels (d–g) are figured. (d) 3D view of the parafoveal TelCap. Note the presence of surrounding string-like (nonfunctional) capillaries. (e) 3D view of the parafoveal collateral vein (blue arrowheads). (f) Abnormal collagen IV labeling over a vein. (g) A venous confluence with one branch occluded (red asterisk). Scale bars: (b, c): 500 μm , d–g: 50 μm .

determines the visual consequences of BRVO, leads to a complex pattern combining capillary closures and focal capillary dilations (Hirano et al., 2021). Such remodeling is double-edged; it may contribute to improve circulation thanks to the development of collateral vessels diverting venous flow from the occluded area; on the opposite, it may exacerbate the visual consequences of BRVO through capillary closure leading to ischemia or rupture of the blood-retinal barrier leading to macular edema. Clinically, post-BRVO microvascular remodeling shares common aspects with diabetic retinopathy, in particular the presence of focal capillary dilations and capillary occlusions. The presence of collateral circulation is a distinguishing feature of retinal vein occlusions.

There have been few histopathological reports of post-BRVO remodeling (Bek, 1998; Bowers et al., 1987; Frangieh et al., 1982; Kimura et al., 2006). In these studies, several types and sizes of microaneurysms have been described ranging from endothelial proliferation to deposits and aggregates of red blood cells and loss of endothelial cells. Occluded capillaries containing a mix of collagenous and lipidic material have been described. Glial cells were reported to contribute to capillary occlusion (Bek, 1998).

In recent years the presence of large capillary abnormalities received increased interest by clinicians because of the recognition of their role in macular edema in eyes with retinal vascular diseases (Bourhis et al., 2010). In particular, it has been shown that targeted photocoagulation of these lesions may contribute to treating macular edema (Ogura et al., 2015; Roh et al., 2021, Paques) and thus appears as a major site of blood-retinal barrier rupture. They are indeed particularly frequent in presence of hard exudates, a marker of the severity of blood-retinal barrier rupture. On the basis of *in vivo* imaging, Cousins et al. (1990) termed capillary macroaneurysms the largest ones. We recently proposed the term telangiectatic capillaries (TelCaps) (Castro Farías et al., 2020) to account for the spectrum of their clinical presentations. Here we report the histopathology of the macula of a donor eye that had a post-BRVO microvascular remodeling, comprising a TelCap.

2 | MATERIAL AND METHODS

The donor was a 91-year-old woman who had an occlusion of the supero-temporal vein of the right eye diagnosed 2 years before death. Due to the presence of a macular edema, she received multiple intravitreal injections of Bevacizumab. Additionally, she had early (dry) AMD. Her medical history also comprised arterial hypertension, hypercholesterolemia, breast and skin cancer, sleep apnea, atrial fibrillation, and stroke. The eye was sampled 16 h post-mortem

in Lion's Gift of Sight bank, accredited by the Eye Bank Association of America and the Food and Drug Administration (FDA). The eye was opened around the ora serrata and fixated in 4% paraformaldehyde (15,710, ThermoFisher Scientific) overnight until processing. Importation in France was done under relevant regulations (CODECOH DC-2015-2400). Upon reception, eyes were examined visually under a binocular microscope to make a post-mortem diagnosis. Microvascular changes seen under the binocular microscope facilitated the identification of the area of interest in the superotemporal quadrant, which was subsequently dissected and processed.

Phosphate buffer saline gelatine triton (PBSGT; 1X PBS containing 0.2% gelatin: 24350262, Prolabo, and 0.5% Triton X-100: X100-500ml, Merck Millipore Sigma–Aldrich) was used for permeabilization and to block non-specific binding sites for 2 h. Immunostaining was realized at 37°C for 24 h, in PBSGT+1 mM Saponin (Merck Millipore Sigma Aldrich S4521). Staining was realized with a mouse primary antibody anti-Collagen IV (CollIV)(Biorad 134,001), a rabbit primary antibody anti-alpha-smooth muscle cell actin (αSMA) (Merck Millipore Sigma Aldrich A2547), and a goat primary antibody anti-von Willebrand Factor (vWF)(Dako A0082, 6.2 $\mu\text{g}/\text{ml}$) antibodies. After washing (PBS, three times), secondary antibodies (Cross-Adsorbed Secondary Antibodies from ThermoFisher) and Hoechst 33342 were incubated in PBSGT+Saponin overnight at 37°C, protected from the light. The secondary antibodies chosen were the following: Donkey antibody directed against mouse antibodies coupled with Alexa647 fluorophore, donkey antibody directed against rabbit antibodies coupled with Alexa546 fluorophore, and donkey antibody directed against goat antibodies coupled with Alexa488 fluorophore. This choice allowed us to specifically stain each antigen of interest (αSMA , CollIV, and vWF) with a different fluorophore, with minimal overlapping of the excitation and emission fluorescence bandwidths, and by doing so to easily separate the fluorescence signals from the different structures. The retina was then washed in PBS and mounted in Vectashield (H1000, Vector Laboratories) for confocal imaging.

Anatomical description of blood vessels distinguishes from outside to inside: the adventitia, media, and intima. Antibodies targeting Collagen IV label preferentially the adventitia. Alpha smooth muscle actin (αSMA) highlights the smooth muscle cells of the media with arteries containing a denser coverage of smooth muscle cells than veins. The intima is made of endothelial cells with elongated nuclei parallel to the vessel axis and storage organelles called Weibel-Palade bodies (WPb). WPb undergoes exocytosis under stress, resulting in platelet adhesion to the endothelium and the sub-endothelial matrix, in particular through the binding of platelets to CollIV (Henrita van Zanten et al., 1996; Saelman et al., 1994).

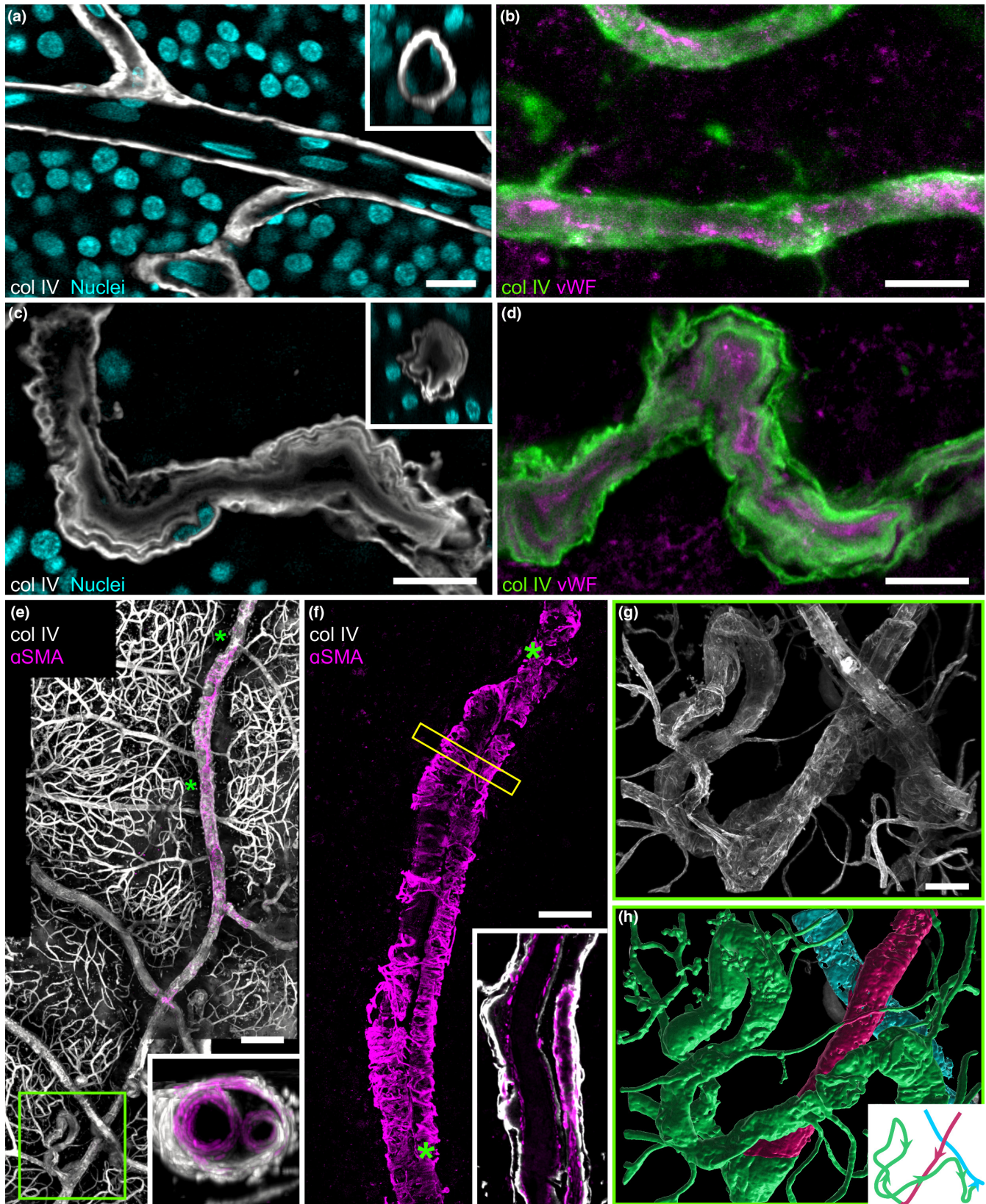


FIGURE 2 (a, b) Optical section of a normal capillary in the unaffected territory. Note the presence of elongated nuclei on the luminal side, typical of endothelial cell nuclei (insert: Cross-section showing its location in the lumen). (c, d) Optical section of a collateral vein showing a thickened, multilayered wall and the absence of nuclear staining. (e, f) Arteriole showing a double channel (green stars: Extremities of the double channel, which is on the right of the artery). (f) α SMA staining of the arteriole. Inserts are optical sections (xz and xy) showing the double channels. (g, h) Arteriovenous communication (green box in (e)), (g) 3D reconstruction of anti-colIV staining. (h) Modeling of the communication shown in (g) (red: Artery, blue: Vein, green: Arteriovenous communication). Scale bars a to d: 20 μ m; e: 100 μ m, f, g: 50 μ m.

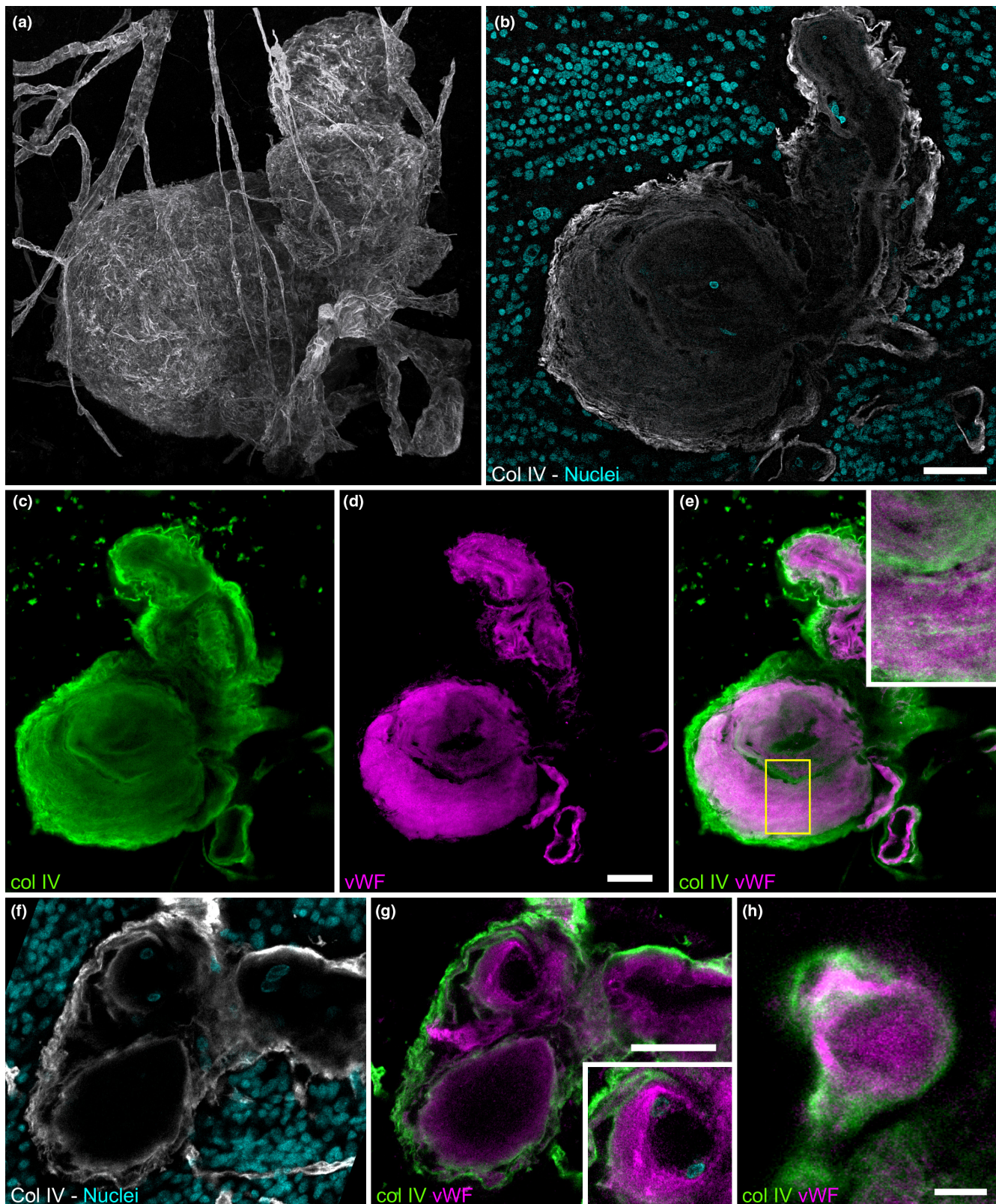


FIGURE 3 (a) 3D-reconstruction of the parafoveal TelCap. Note that string-like collagen IV positive structures surround the lesion, suggestive of capillary remnants. (b) Optical section revealing a multilayered, thickened wall concentric to a small lumen. Few nuclei are seen on the luminal side. (c–e) Staining of col IV and vWF. Note the onion-like pattern of ColIV and vWF. (f, g) Optical sectioning of a medium-sized focal dilation. The insert superimposes the nuclei staining, showing presumed endothelial cells lining the lumen and the vWF accumulation external to the cells. (h) Small capillary dilation with vWF-containing material filling the lumen. Scale bar: a, b: 100 μm, c to g: 50 μm, h: 10 μm.

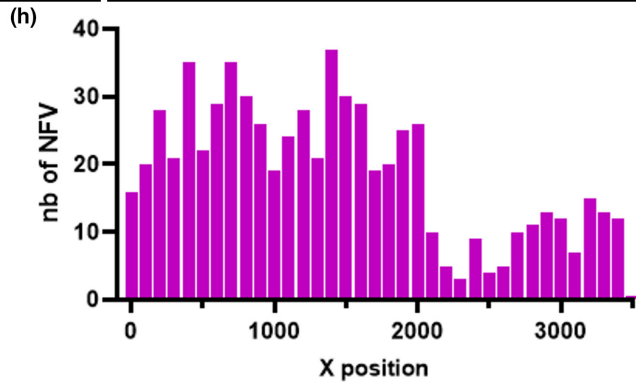
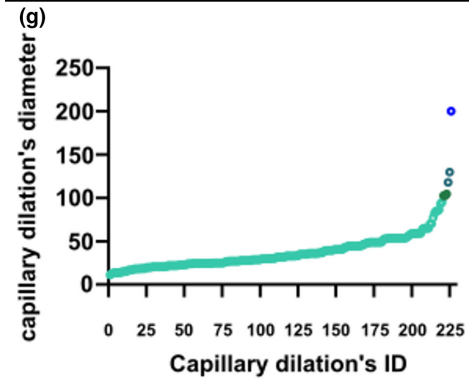
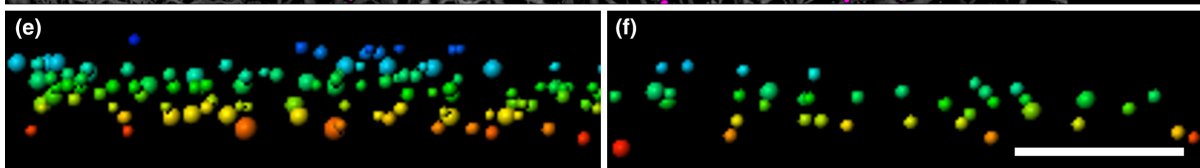
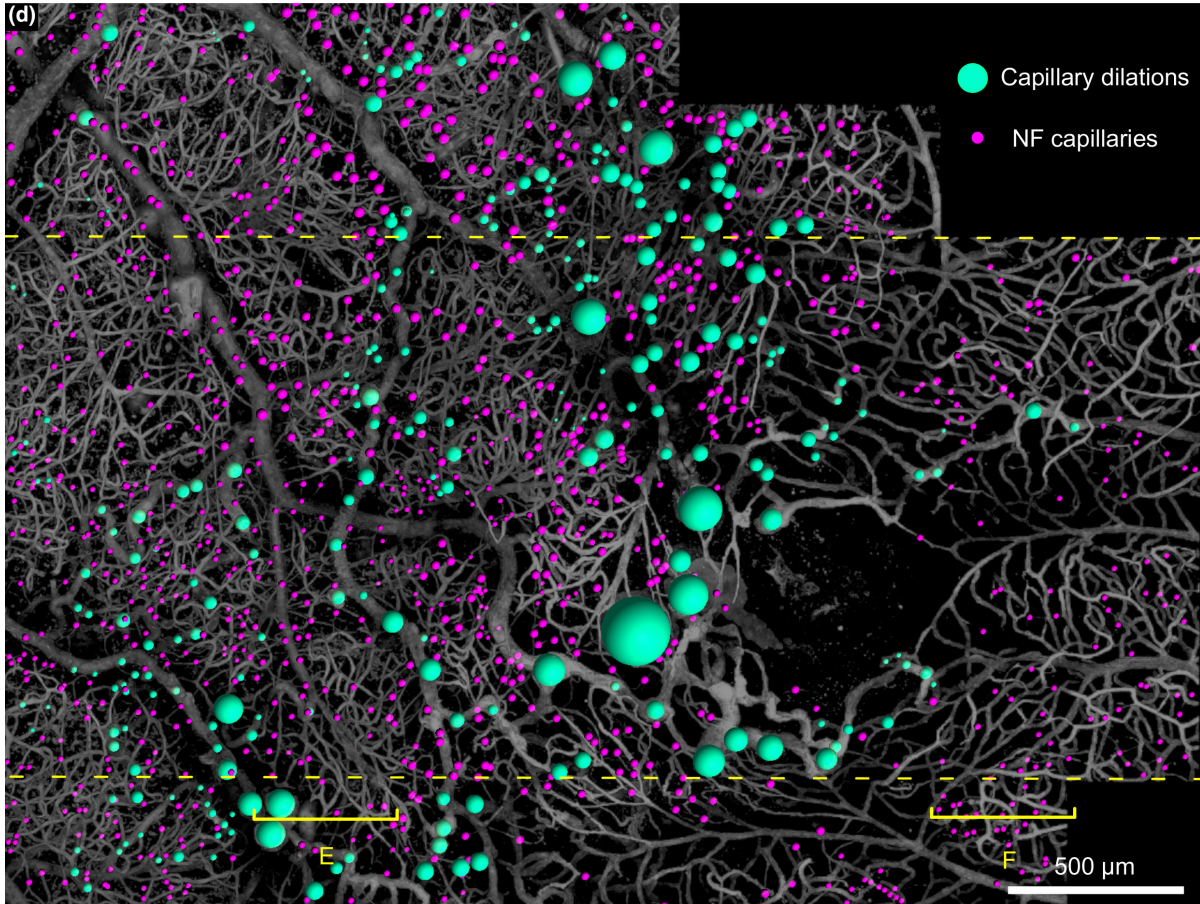
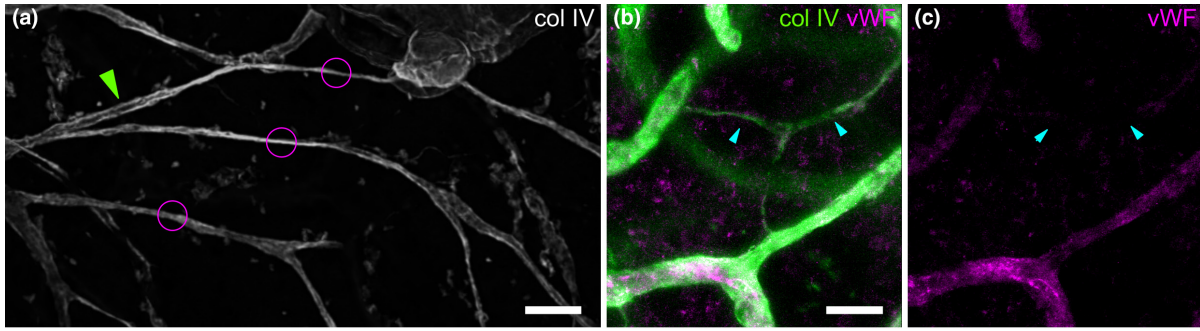


FIGURE 4 (a–c) Confocal microscopy of non-functional capillaries. (a) Example of capillaries remnants. (b, c) Absence of vWF staining of capillary remnants. (d) Mapping of capillary dilations and nonfunctional capillaries in the whole sample. (e, f) XZ distribution of capillary dilations and nonfunctional capillaries in affected retina versus the unaffected retina from the cross-sections (sampling zone shown by the yellow bracket in (d); inner retina is on top; color coding is for distinguishing the level in the z axis). (g) Diameter of capillary dilations was ordered by size. (h) Frequency histogram of nonfunctional capillaries (NFV) within the dashed yellow lines in (d)). Scale bar: a to c, 20 μm d 500 μm , e, f: 100 μm .

Immunofluorescence images were acquired with either an epifluorescence microscope (Leica DM5500 B) or a confocal microscope, with an oil or silicon immersion objective (Olympus, FV1000). Epifluorescence microscopy confirmed the identification of the area of interest. Images and 3D volumes were generated with FIJI and Imaris x64 software (version 8.4.1 and 9.2.1 Bitplane). Whenever necessary, deconvolution was realized through Imaris 'image processing plugin. Stack images were first converted to imaris files (.ims) with ImarisFileConverter, and 3D reconstruction was performed with the volume rendering function. Optical slices in different axes were obtained with the ortho slicer tool. The surface tool was manually applied with the selection of the mask option to isolate the individual structure or remove the signal from the inner limiting membrane. 3D pictures and movies were generated with the snapshot and animation tools. Figures were assembled using FIJI and the Scientifig plugin.

3 | RESULTS

The post-mortem fundus photograph (Figure 1a) shows the area examined by confocal microscopy (Figure 1c) which measured 3.5 \times 2.7 mm. Overview of the sample by epifluorescence microscopy with CollIV staining (Figure 1b) revealed disseminated microvascular abnormalities. Around the foveal avascular zone (FAZ), a large capillary dilation was present (Figure 1d and Figure 2). A collateral vessel was also seen passing through the perifoveal arcade (Figure 1e, detailed in Figure 3). There were no areas devoid of capillary structures; instead, in affected areas, we found numerous micrometer-wide, collIV positive, vWF negative strings connected to the vascular network. They were all negative for Hoechst staining. They were thus assumed to be remnants of nonperfused capillaries and subsequently termed nonfunctional (NF) capillaries. Other vascular abnormalities such as pathological CollIV pattern (Figure 1f) or veins occluded by collagen walls (Figure 1g) were found. Collateral vessels passing through the median raphe encroached the inferotemporal area. The video can be seen at <https://histo.pariseyeimaging.com/Resources/ab075ea7d1-Confocal-microscopy-of-telangiectatic-capillaries-%28TelCaps%29-and-other-features-of-microvascular-remodeling-following-BRVO.en.htm>.

Figure 2a,b are confocal microscopy images of normal retinal vessels, i.e., located outside of the retinal quadrant affected by BRVO. They show a thin collagen wall and a lumen lined by elongated nuclei of endothelial cells (Figure 2a) and granular labeling of vWF (Figure 2b) similar to what is expected from normal vessels. Comparatively, the collateral vein of the perifoveal arcade (Figure 2c,d) shows no cell nuclei in the lumen (Figure 2c), and the vWF staining was located inside the lumen (2d), most likely corresponding to vWF deposits.

Vascular remodeling was also observed in arteries. Figure 2e,f shows an artery in which a 450 μm long segment is duplicated. Both channels present a lumen surrounded by a layer of smooth muscle cells and a weakly stained collagen sheath, included within a single collagenous sheath. Nuclear staining suggestive of endothelial cells was present, but not vWF staining (not shown). A dilated capillary connection between arteriole and venule was found (Figure 2g,h), suggesting that arteriovenous shunting through a dilated capillary may have contributed to nonperfusion.

Capillary and venous dilations of varying sizes and shapes were found throughout the affected area and encroached on the unaffected area. Some were small focal bulges, in particular in collateral vessels (Figure 3h). A variety of sizes and shapes was observed: saccular, peduncular, irregular, or polylobulated. Their diameters ranged from 10 μm to hundreds of μm . All types of capillary dilations showed vWF staining, while most were devoid of Hoechst staining on their intraluminal side, indicating paucicellularity and hence extensive loss of endothelial cells (Figure 2g). All capillary dilations were surrounded by nonfunctional capillaries. Some small microaneurysms were occluded by vWF-containing material (Figure 2H). The largest one was found adjacent to the fovea (Figure 2a), connected to a collateral vessel passing in the perifoveal arcade. It was a polylobular capillary dilation, measuring 233 μm in its largest diameter, and 110 μm in thickness, hence fitting the clinical description of TelCaps. The TelCap was surrounded by non-functional capillaries. Optical sectioning did not reveal a consistent lumen (Figure 2b), that is, a channel passing through the entire lesion. The TelCap was paucicellular as shown by Hoeschst staining (Figure 2b). The wall of the lesion was organized in an "onion layers" pattern expressing collagen IV and vWF (2c–e). Since the vessels closest to the fovea are capillaries, it can be assumed that the perifoveal telangiectasis and collateral vessels both emerged from capillaries.

Nonfunctional capillaries, that is, CollIV-positive linear structures thinner than expected for capillaries (Figure 4a,b), without vWF or nuclear staining and without a continuous lumen were found throughout the affected area (Figure 4d,h) throughout the retinal thickness (Figure 4e,f). Capillary dilations were similarly distributed. When ordering capillary dilations by size, it appears that the largest one was an outlier (Figure 4g) suggesting that the growth of small lesions and TelCaps may be driven by different factors.

4 | DISCUSSION

BRVO may spark chronic remodeling of retinal microvessels that may comprise neovessels but also non-neovascular changes such as capillary dilation, capillary closure, and collateral vessels (also

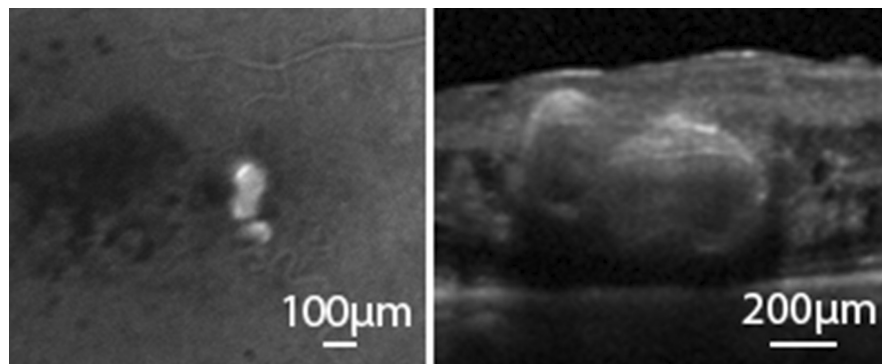


FIGURE 5 Clinical imaging of a TelCap. Left: In vivo late frame of ICG angiography in a patient showing staining of a TelCap. Right: OCT through the same TelCap showing the hyperreflective thickened wall.

termed shunt vessels). As already reported by clinical imaging (Dubow et al., 2014), we found in our case a wide spectrum of pathological microvascular phenotypes, with capillary dilations displaying a wide variety of shapes and sizes. In the smallest ones, the dilation appears as a thin-walled bulge of intramural vWF deposit with endothelial cells lining the vessels. With increasing size, the collagen wall was thicker, multilayered, and endothelial cells less numerous. In the largest ones, vWF was present through the entire wall, intercalated with ColIV in an onion-like pattern; the wall-to-lumen ratio was higher than in smaller lesions, and there were very few endothelial cells.

As previously reported (Kimura et al., 2006; Stitt et al., 1995) few endothelial cells were found in the lumen of capillary dilations. As endothelial cells play a fundamental role in capillary homeostasis, it can be hypothesized that these de-endothelialized capillary tubes would favor local thrombosis. Furthermore, since endothelial cells are also effectors of the BRB, there is likely a rupture of the BRB. Unfortunately, for this case study, we do not have clinical imaging to ascertain the presence of flow or focal BRB rupture in these de-endothelialized vessels. Our finding of a generalized loss of endothelial cells suggests that the mechanisms of capillary bulges in RVO may be different from that of microaneurysms in diabetic retinopathy, in which local proliferation of endothelial cells has been noted (Moore et al., 1999). Also, diabetic retinopathy is largely restricted to capillaries, while BRVO may affect pre and post-capillary vessels as well.

Since vWF may either be intracytoplasmic or released into the plasma, the interpretation of anti-vWF staining in diseased tissue may be ambiguous. Indeed, the lack of anti-vWF staining may indicate the release of WPB and hence not necessarily endothelial cell death; on the contrary, diffuse vWF staining may be due to plasma deposition on the subendothelial matrix. We were limited in the number of antibodies that could be used, consequently, we could not detect the presence of endothelial-cell-specific antigens such as VCAM. However, nuclear staining was consistently decreased or absent in affected vessels, hence we are confident that there were few to no endothelial cells present. Therefore, we conclude that vWF staining in diseased areas was not related to the presence of endothelial cells, but was indeed most likely due

to plasma deposition. Moreover, the pattern of diffuse vWF staining was different from the granular pattern of healthy endothelial cells. Intraluminal deposition of material in capillary dilations has been observed by electron microscopy in microaneurysms. Such material was identified as either stagnant blood, lipids, fibrin (Ashton, 1963; Stitt et al., 1995), or vWF (Moore et al., 1999). Some reports previously mentioned the presence of a multilayered pattern of vascular wall thickening (Stitt et al., 1995). Ezra et al. (2013) postulated that a higher vWF staining is a marker of a higher risk of microaneurysm leakage, independently of size. We show here that vWF deposition may be intermixed with collagen IV, suggesting that both plasma deposition of vWf and extracellular matrix synthesis contribute to the wall thickening. Since capillary dilations contained only a few nuclei, the source of collagen synthesis and vWF in the lumen is uncertain. If plasma deposition is indeed the source of parietal vWf, this would mean, in return, that de-endothelialized capillaries can conduct blood flow.

Non-functional capillary remnants, which have also been called capillary ghosts, were numerous; no retinal area devoid of them was found. This shows that following occlusion, the collagen scaffold of capillaries persists. The cause of capillary occlusion during retinal vascular diseases remains uncertain. We observed dilated capillaries causing what is likely a shunt effect (Figure 3h), which may have contributed to capillary nonperfusion. Another case showed complete filling by vWf-positive material. We also documented occluded veins, in particular a venous confluence in which one of the branches was obturated by collagen. Whether these processes are the actual cause or a consequence of capillary nonperfusion remains to be determined.

We analyzed the largest capillary dilation, which was a 233µm wide parafoveal lesion. Despite the exponential development of clinical imaging exemplified by optical coherence tomography angiography (Hamada et al., 2018), there is still a lack of a clear definition of TelCaps that could guide therapeutic choices. Clinically, it has been proposed that the distinction of Telcaps from microaneurysms be based on their clinical imaging characteristics, mainly their larger size and their elective, persistent staining by the intravitral dye indocyanine green (ICG) (example unrelated to this case is shown in Figure 5). To our knowledge, this is the first detailed

histopathological report of a lesion that meets the clinical criteria of a TelCap, that is, a capillary lesion of more than 100 microns (Cousins et al., 1990). However, we are unaware of previous ICG angiography in our patient, which is an important diagnostic marker of TelCaps. Nevertheless, our histopathological findings may contribute to a better understanding of the characteristics and causes of telcaps. We found that instead of a clear-cut structural distinction between micro and macroaneurysm, there is a continuum of structural changes from small bulges of venules to TelCaps, yet the largest lesions were clearly outliers in size compared to the other lesions. This supports the definition of post-BRVO telcaps by their size. However, other than the outer diameter, a possible distinctive structural element between telcaps and microaneurysms could be a higher wall-to-lumen ratio. The presence of vWf may account for the ICG staining, yet such vWf was widely distributed and hence cannot solely account for ICG staining of TelCaps. The multilayered pattern of the thickened wall fits with their aspect by in vivo optical coherence tomography. Given the fact that the wall of the telcap was almost completely obturated by the thickened wall, spontaneous occlusion of a TelCap may, therefore, result from a thrombosis but also from obliteration due to an increase of the thickness of its wall.

To sum up, we describe the spectrum of microvascular abnormalities upstream of a longstanding BRVO. This spectrum comprises a large parafoveal telangiectatic capillary corresponding to what has been previously clinically defined as TelCap. The absence of intraluminal nuclear staining in the majority of abnormal vessels raises the hypothesis that the loss of endothelial cells plays a crucial role in the development of the different manifestations of capillary remodeling. The presence of vWF in de-endothelialized vessels suggests deposition of plasma, hence, they may remain perfused. Our work may help to understand the clinical imaging features of TelCaps.

ACKNOWLEDGMENT

We would like to thank Nathaniel Norberg for his proofreading and advice.

FUNDING INFORMATION

Région Ile-De-France (EX047007 - SESAME 2019-4DEye), Programme d'Investissements d'Avenir of the French state (Agence Nationale de la Recherche [ANR-18-IAHU-01 ForeSight]) and the Association contre l'OVR.

DATA AVAILABILITY STATEMENT

Data are available on request from the authors.

ORCID

Marie Darche  <https://orcid.org/0000-0001-9065-2528>

REFERENCES

- Ashton, N. (1963) Studies of the retinal capillaries in relation to diabetic and other retinopathies. *The British Journal of Ophthalmology*, 47, 521–538.
- Bek, T. (1998) Capillary closure secondary to retinal vein occlusion. A morphological, histopathological, and immunohistochemical study. *Acta Ophthalmologica Scandinavica*, 76(6), 643–648. <https://doi.org/10.1034/j.1600-0420.1998.760601.x>
- Bourhis, A., Girmens, J.F., Boni, S., Pecha, F., Favard, C., Sahel, J.A. et al. (2010) Imaging of macroaneurysms occurring during retinal vein occlusion and diabetic retinopathy by indocyanine green angiography and high resolution optical coherence tomography. *Graefes' Archive for Clinical and Experimental Ophthalmology*, 248, 161–166.
- Bowers, D.K., Finkelstein, D., Wolff, S.M. & Green, W.R. (1987) Branch retinal vein occlusion. *A Clinicopathologic Case Report Retina*, 7(4), 252–259. <https://doi.org/10.1097/00006982-198707040-00011>
- Castro Fariás, D., Matsui Serrano, R., Bianchi Gancharov, J., de Dios, C.U., Sahel, J., Graue Wiechers, F. et al. (2020) Indocyanine green angiography for identifying telangiectatic capillaries in diabetic macular oedema. *The British Journal of Ophthalmology*, 104(4), 509–513.
- Cousins, S.W., Flynn, H.W., Jr. & Clarkson, J.G. (1990) Macroaneurysms associated with retinal branch vein occlusion. *American Journal of Ophthalmology*, 109(5), 567–570. [https://doi.org/10.1016/s0002-9394\(14\)70687-7](https://doi.org/10.1016/s0002-9394(14)70687-7) PMID: 2333919.
- Dubow, M., Pinhas, A., Shah, N. et al. (2014) Classification of human retinal microaneurysms using adaptive optics scanning light ophthalmoscope fluorescein angiography. *Investigative Ophthalmology & Visual Science*, 55, 1299–1309.
- Ezra, E., Keinan, E., Mandel, Y., Boulton, M.E. & Nahmias, Y. (2013) Non-dimensional analysis of retinal microaneurysms: critical threshold for treatment. *Integr Biol (Camb)*, 5(3), 474–480.
- Frangieh, G.T., Green, W.R., Barraquer-Somers, E. & Finkelstein, D. (1982) Histopathologic study of nine branch retinal vein occlusions. *Archives of Ophthalmology*, 100(7), 1132–1140. <https://doi.org/10.1001/archophth.1982.01030040110020>
- Hamada, M., Ohkoshi, K., Inagaki, K. et al. (2018) Visualization of microaneurysms using optical coherence tomography angiography: comparison of OCTA en face, OCT B-scan, OCT en face, FA, and la images. *Japanese Journal of Ophthalmology*, 62, 168–175.
- Henrita van Zanten, G., Saelman, E.U., Schut-Hese, K.M., Wu, Y.P., Slootweg, P.J., Nieuwenhuis, H.K. et al. (1996) Platelet adhesion to collagen type IV under flow conditions. *Blood*, 88(10), 3862–3871.
- Hirano, Y., Suzuki, N., Tomiyasu, T. et al. (2021) Multimodal imaging of microvascular abnormalities in retinal vein occlusion. *Journal of Clinical Medicine*, 10(3), 405. <https://doi.org/10.3390/jcm10030405>
- Kimura, T., Mizota, A., Adachi-Usami, E., Tsuyama, Y. & Fujimoto, N. (2006) Histopathological study of a case with branch retinal vein occlusion. *Annals of Ophthalmology (Skokie, Ill.)*, 38(1), 73–76. <https://doi.org/10.1385/ao:38:1:73>
- Moore J, Bagley S, Ireland G, McLeod D, Boulton ME. Three dimensional analysis of microaneurysms in the human diabetic retina. *Journal of Anatomy* 1999;194 (Pt 1):89–100. doi: <https://doi.org/10.1046/j.1469-7580.1999.19410089.x>.
- Ogura, S., Yasukawa, T., Kato, A., Kuwayama, S., Hamada, S., Hirano, Y. et al. (2015) Indocyanine Green angiography-guided focal laser photocoagulation for diabetic macular edema. *Ophthalmologica*, 234(3), 139–150.
- Roh, H.C., Lee, C., Kang, S.W., Choi, K.J., Eun, J.S. & Hwang, S. (2021) Infrared reflectance image-guided laser photocoagulation of telangiectatic capillaries in persistent diabetic macular edema. *Scientific Reports*, 11(1), 21769.
- Saelman, E.U., Nieuwenhuis, H.K., Hese, K.M., de Groot, P.G., Heijnen, H.F., Sage, E.H. et al. (1994) Platelet adhesion to collagen types I through VIII under conditions of stasis and flow

is mediated by GPIa/IIa (alpha 2 beta 1-integrin). *Blood*, 83(5), 1244–1250.

- Song, P., Xu, Y., Zha, M., Zhang, Y. & Rudan, I. (2019) Global epidemiology of retinal vein occlusion: a systematic review and meta-analysis of prevalence, incidence, and risk factors. *Journal of Global Health*, 9(1), 010427. <https://doi.org/10.7189/jogh.09.010427>
- Stitt, A.W., Gardiner, T.A. & Archer, D.B. (1995) Histological and ultrastructural investigation of retinal microaneurysm development in diabetic patients. *The British Journal of Ophthalmology*, 79, 362–367.

How to cite this article: Darche, M., Verschueren, A., Castro Farias, D., Borella, Y. & Paques, M. (2023) Confocal microscopy of telangiectatic capillaries (TelCaps) and other features of microvascular remodeling following branch retinal vein occlusion. *Journal of Anatomy*, 243, 235–244. Available from: <https://doi.org/10.1111/joa.13743>